Gamma photons and electron-positron pairs from ultra-intense laser-matter interaction: A comparative study of proposed configurations

View Online   Export Citation   CrossMark

Yan-Jun Gu,[1,2,a)] (iD) Martin Jirka,[1,3] Ondrej Klimo,[1,3] (iD) and Stefan Weber[1,4]

AFFILIATIONS

[1]Institute of Physics of the ASCR, ELI-Beamlines, Na Slovance 2, 18221 Prague, Czech Republic
[2]Institute of Plasma Physics of the CAS, Za Slovankou 1782/3, 18200 Prague, Czech Republic
[3]FNSPE, Czech Technical University in Prague, 11519 Prague, Czech Republic
[4]School of Science, Xi'an Jiaotong University, Xi'an 710049 China

[a)]**Electronic mail:** yanjun.gu@eli-beams.eu

ABSTRACT

High-energy γ-photon generation via nonlinear Compton scattering and electron–positron pair creation via the Breit–Wheeler process driven by laser–plasma interaction are modeled, and a number of mechanisms are proposed. Owing to the small cross section, these processes require both an ultra-intense laser field and a relativistic electron bunch. The extreme conditions for such scenarios can be achieved through recent developments in laser technology. Photon emission via nonlinear Thomson and Compton scattering has been observed experimentally. High-energy positron beams generated via a multiphoton process have recently been observed too. This paper reviews the principles of γ-ray emission and e^+e^- pair creation in the context of laser–plasma interaction. Several proposed experimental setups for γ-ray emission and e^+e^- pair creation by ultra-intense laser pulses are compared in terms of their efficiency and the quality of the γ-photon and positron beams produced for ultrashort (15 fs) and longer (150 fs) multi-petawatt laser beams.

I. INTRODUCTION

The 2018 Nobel Prize in Physics was awarded to Ashkin, Mourou, and Strickland for their groundbreaking inventions in the field of laser physics. The chirped pulse amplification (CPA) technique proposed by Strickland and Mourou[1] provides significantly enhanced laser intensities in excess of 10^{18} W cm^{-2}. The increasing intensity pushes the particle dynamics in the laser field into the relativistic region, thus providing a basis for the development of laser-driven accelerators. Electrons in the plasma with appropriate phases are accelerated to relativistic energies within millimeters by the wakefield or directly by the laser field. Several regimes have been proposed for the production by these relativistic electrons of radiation ranging from X rays to γ rays. State-of-the-art laser facilities[2,3] are able to deliver intensities of the order of 10^{22} W cm^{-2}. The next generation of lasers are designed for the 10 PW region, with the corresponding intensities being expected to reach the order of 10^{23}–10^{24} W cm^{-2} or even higher.[4,5] As a result of interaction with such high-intensity fields, the emitted γ photons have a momentum comparable to the

that of the electrons, and quantum electrodynamic (QED) effects then become significant. Processes generating secondary sources of particles, such as γ-photon emission, electron–positron pair creation, and QED cascades, come into play under these extreme intensity conditions, and the corresponding phenomena have been widely studied.[6–28] Experimental signatures of radiation reaction and QED processes have been reported recently.[29,30]

The regimes for γ-ray emission in laser–plasma interaction include bremsstrahlung, synchrotron emission, nonlinear Thomson scattering, and nonlinear Compton scattering. Bremsstrahlung[31–33] dominates in the case of solid targets at laser intensities below 10^{22} W cm^{-2}. Giulietti et al.[34] reported an intense γ-ray source around the giant dipole resonance for photonuclear absorption obtained via electron-bunch bremsstrahlung driven by a 10 TW laser. Vyskočil et al.[35] described γ-ray emission in laser–foil interactions using kinetic simulations and found that the corresponding γ-ray spectra show a linear dependence of the γ-ray temperature on the normalized laser potential. With high-energy electron beams, γ photons can be obtained via nonlinear

Thomson scattering. Sarri *et al.*[36] reported experimental observations of ultrahigh-brilliance [10^{20} s^{-1} mm^{-2} mrad^{-2} (0.1%BW)$^{-1}$] multi-MeV γ rays from nonlinear relativistic Thomson scattering. High-energy electrons in the self-generated magnetic field emit multi-MeV photons, as described by Stark *et al.*[37] Yan *et al.*[38] presented measurements of high-order multiphoton Thomson scattering from a laser-driven electron beam. Recently, solid nanowires have been reported to be ideal materials for γ-ray generation. Martinez *et al.*[39] presented a numerical study of the synchrotron emission resulting from the interaction of a strong laser field with a nanowire array. Wang *et al.*[40] proposed the use of an electron wiggling regime to obtain collimated γ rays along a petawatt laser-irradiated wire. Nonlinear Compton scattering[41,42] is the main mechanism for γ-ray production in the case of relativistic electrons interacting with ultra-intense electromagnetic (EM) fields. Chang *et al.*[20] proposed the use of circularly polarized laser pulses to produce photon emission with high brightness in a plasma channel. According to Benedetti *et al.*,[43] collimated γ-ray flashes with high brilliance [10^{25} s^{-1} mm^{-2} mrad^{-2} (0.1%BW)$^{-1}$] are obtained via plasma filaments as a result of synchrotron emission from an ultra-relativistic electron bunch traveling in a millimeter-scale conductor. Recently, high-order Laguerre–Gaussian mode laser and compound targets[44] have been used to induce nonlinear Compton scattering. A tunable γ-ray beam generation regime using an oscillating plasma mirror has also been proposed recently.[45] In the case of an extremely strong EM field interacting with γ photons, e^+e^- pairs are produced by the multiphoton Breit–Wheeler (BW) process[46,47] $\gamma + n\hbar\omega_0 \rightarrow e^- + e^+$, where ω_0 is the laser frequency and n is the number of laser photons. The small cross section for photon–photon collisions means that the threshold field intensity for BW process can be as high as 10^{24} W cm^{-2}.[7] QED cascades in the multiple counterpropagating regime have been proposed in recent theoretical studies.[9,19,21,48,49] Regimes involving pair creation with a single laser pulse have also been proposed on the basis of a strong electron self-injection effect[18] and circular oscillations in the plasma channel.[50] Normal injection of a multi-PW laser into a bunch of GeV-class electron beams has been reported to produce a low-divergence electron–positron pair beam.[51] A new mechanism based on a relativistic plasma mirror has recently been proposed[52] in which the pair creation efficiency and the production rate are significantly enhanced.

In this paper, we briefly introduce the laser–plasma interaction in the ultrarelativistic regime, together with the corresponding radiation and QED effects. The recent proposed regimes for γ-ray emission and pair creation are reviewed and compared. The scenarios for each setup are presented using particle-in-cell simulations. The advantages and disadvantages of this approach are summarized.

II. GENERAL DESCRIPTION OF ULTRA-INTENSE AND ULTRASHORT LASER–MATTER INTERACTION

The intensity at which the electromagnetic field exceeds the binding strength of an electron to an atom is about $I_a = ce^2/(8\pi a_B^4) \approx 3.5 \times 10^{16}$ W cm^{-2}, where $a_B = \hbar^2/(m_e e^2)$ is the Bohr radius and other physical constants have their usual meanings (c is the speed of light, e the electron charge, m_e the electron mass, and $\hbar$ the reduced Planck's constant). An ultra-intense laser pulse can ionize any target even without account being taken of multiphoton

and tunneling ionization effects, which actually reduce the threshold value to the order of 10^{14} W cm^{-2}. The prepulse or the pedestal of an ultra-intense laser is strong enough to ionize the target material. The strength of the laser pulse is scaled by the dimensionless parameter $a_0 = eE_0/m_e\omega c$, where E_0 is the laser electric field and ω is the angular frequency. The relation between the laser intensity and the normalized amplitude is $a_0 \approx 8.57 \times 10^{-10} \sqrt{I\,(\text{W cm}^{-2})}\,\lambda\,(\mu\text{m})$. Laser–plasma interactions in the intensity range of 10^{18}–10^{23} W cm^{-2} are discussed below.

A. Relativistic laser–plasma interaction and particle acceleration

When the dimensionless amplitude $a_0 = 1$, this means that the field provides work equal to $m_e c^2$ within a distance $\lambda/2\pi$. Relativistic effects must be considered when $a_0 \gg 1$, which implies that the electron can be accelerated to relativistic energy in the distance of one laser period. In such a relativistic laser–plasma interaction, electron thermal motion can be neglected, since it is much weaker than the motion driven by the laser field. The transverse and longitudinal motion of a free electron in a planar laser field satisfies $\boldsymbol{u}_\perp = \boldsymbol{a}$ and $u_\parallel = \gamma - 1 = a_0^2/2$. Here, $\boldsymbol{a} = e\boldsymbol{A}/mc^2$ is the instantaneous normalized vector potential and $\boldsymbol{u}_\perp$ and $u_\parallel$ are respectively the transverse and longitudinal components of the electron momentum normalized by $m_e c$. In the case of $a \gg 1$, the longitudinal momentum is much larger than the transverse momentum. Therefore, the response of an electron to a relativistic laser field is dominated by its longitudinal motion driven by the ponderomotive force. It is also clear that there is no energy gain by an electron passing through a plane wave, since the vector potential is zero before and after the pulse. Energy gain is possible, for example, with a focused laser pulse in which the electron experiences different field strengths at different distances from the focal point.

Based on single-electron dynamics, we discuss the interaction of a laser and an underdense plasma with a density lower than the critical density $n_{cr} = m_e\omega^2/4\pi e^2$. A plasma with electron density higher than the critical density becomes opaque to an EM field with frequency ω. Taking the relativistically induced transparency effect into account, the cutoff density is increased to γn_{cr} as the electron mass increases by the Lorentz factor γ. The ponderomotive force of the laser field propagating in an underdense plasma and the restoring electrostatic force in the plasma provide the possibility of creating a large-amplitude wakefield. This laser wakefield excitation is an important process in which electrons can be trapped and accelerated in an efficient way. A sinusoidal type of density perturbation $\delta n/n_0$ is induced by a laser pulse in a plasma with an initial density of n_0. The perturbations are accompanied by an electrostatic field (wakefield) with maximum amplitude $E_{max} \sim \sqrt{2(\gamma-1)}$.[53] When the optimal conditions are satisfied, the maximum energy gain for the electrons trapped inside the wakefield is proportional to $\gamma \propto c\tau\sqrt{P_L}$, where τ and P_L are the pulse length and peak power of the laser.

Electrons in the plasma can also be trapped by the laser field and heated via the direct laser acceleration (DLA) mechanism.[54] In this case, the electrons experience betatron oscillations in the transverse direction driven by the laser field. In the ultrarelativistic case, the electric and magnetic components of the Lorentz force are of the same order of magnitude, since the corresponding transverse velocity is of the order of the speed of light. The electrons are accelerated by the

$u_\perp/\gamma \times B$ force in the longitudinal direction and comoving with the laser field.

B. Radiation reaction and QED

With increasing intensity and particle energy, the charged particle dynamics becomes dissipative owing to the emission of high-energy photons. Here, we introduce a dimensionless parameter $\epsilon_{\text{rad}} = 4\pi r_e/3\lambda$, where $r_e = e^2/m_e c^2$ is the classical electron radius. Nonlinear Thomson scattering has emission power proportional to the fourth power of the electron energy: $P_\gamma \approx \epsilon_{\text{rad}} m_e c^2 \omega \gamma^4$. Radiation effects become important when the energy gain per unit time ($P_e = a_0 \omega m_e c^2$) is balanced by the radiation loss, i.e., $a_0 > \epsilon_{\text{rad}}^{-1/3}$. The corresponding laser intensity is $I_R \approx 2.65 \times 10^{23}(1\,\mu m/\lambda)^{4/3}$ W cm^{-2}.[55] The electron dynamics is significantly affected by the radiation reaction due to the recoil momentum from the emitted photons, which is equivalent to the radiation damping force in the Landau–Lifshitz form[56] $F_{rr} \approx -(2e^4/3m_e^2 c^5)\gamma^2 v[(E + v \times B/c)^2 - (E \cdot v)^2/c^2]$. In the case of the electron DLA mechanism, the radiation damping force prevents the electrons from escaping from the pulse center.

When the emitted photon energy is comparable to the electron kinetic energy, i.e., $\hbar\omega_\gamma \approx \gamma_e m_e c^2$, QED effects must be taken into account. The threshold for these effects is determined by the dimensionless relativistic and gauge-invariant parameter $\chi_e = \sqrt{(F^{\mu\nu}p_\mu)^2}/(E_s m_e c)$, where $F^{\mu\nu} = \partial_\mu A_\nu - \partial_\nu A_\mu$ is the 4-tensor of the EM field, p_ν is the electron 4-momentum, and $E_s = m_e^2 c^3/e\hbar$ is the critical QED electric field, i.e., the Schwinger limit field. In the case of a plane EM wave, the invariant parameter can be expressed as $\chi_e = (E/E_s)(\gamma - p_\parallel/m_e c)$. Considering $\gamma \gg 1$ under the ultrarelativistic condition, the corresponding parameter is maximized in a counterpropagating geometry of EM field and electrons, $\chi_e^{\uparrow\downarrow} \approx 2\gamma(E/E_s)$. However in the copropagating case, it dramatically decreases to $\chi_e^{\uparrow\uparrow} \approx (2\gamma)^{-1}(E/E_s)$.

High energy photons produce e^+e^- pairs in the extremely strong field via the multiphoton BW process $\gamma + n\hbar\omega \rightarrow e^- + e^+$. An important parameter in calculating the probability of this QED process is $\chi_\gamma = \sqrt{(F^{\mu\nu}k_\nu)^2}/(E_s m_e c)$, where $\hbar k_\nu = (\hbar\omega_\gamma, \hbar \mathbf{k}_\gamma)$ is the 4-momentum of the high-energy photon. It can be expressed in the three-dimensional geometry as

$$\chi_\gamma = \frac{1}{E_s}\sqrt{\left(\frac{\hbar\omega_\gamma E}{m_e c^2} + \frac{\mathbf{k}_\gamma \times B}{m_e c}\right)^2 - \left(\frac{\mathbf{k}_\gamma \cdot E}{m_e c}\right)^2}.$$

Similar to the case of γ-photon emission discussed above, χ_γ can be calculated in the case of photons interacting with the plane EM field: $\chi_\gamma = (E/E_s)(\hbar\omega - k_\parallel c)/m_e c^2$. The counterpropagating and copropagating photons have $\chi_\gamma^{\uparrow\downarrow} \approx 2(\hbar\omega/m_e c^2)(E/E_s)$ and $\chi_\gamma^{\uparrow\uparrow} \approx 0$, respectively.

III. MECHANISMS OF γ-RAY AND ELECTRON–POSITRON PAIR PRODUCTION

In this section, we review several recently proposed mechanisms for generating γ rays and e^+e^- pairs. As mentioned above, the probabilities for γ-ray emission and e^+e^- pair creation are both inversely proportional to the Schwinger limit field $E_s \approx 1.32 \times 10^{18}$ V m^{-1}.

Assuming that the electric field strength reaches $\sim 10^{15}$ V m^{-1}, corresponding to a laser intensity of 10^{24} W cm^{-2}, the ratio $E/E_s \sim 10^{-3}$. This implies that the cross sections for the QED processes are still exponentially small. The way to increase the parameters χ_e and χ_γ to $\chi_{e,\gamma} \sim 1$ is to use an optimal geometry and enhance the energy of the electrons and the photons. To satisfy the optimal conditions, various setups have been proposed and studied intensively in recent years. We classify these mechanisms according to the setup and summarize the achievements. For each category, we present our simulations using the 2D PIC code EPOCH[57,58] to illustrate the main results. The laser wavelength $\lambda = 1\,\mu m$ and the power chosen in the simulations is 70 PW for the mechanism employing a single pulse or 35 PW in the case of two laser pulses. The focal spot size is 3 μm, and thus the peak laser intensities are 5×10^{23} W cm^{-2} and 2.5×10^{23} W cm^{-2}, respectively. Two different pulse lengths are compared for each mechanism: a short pulse of 15 fs and a long pulse of 150 fs.

A. Multicolliding laser pulses

Pair creation by multicolliding pulses in vacuum was proposed in Ref. 9, where it was theoretically predicted that the pair creation threshold could be reduced by concentrating the EM field energy into a small volume. Since then, there have been several presentations of the use of multiple counterpropagating pulses interacting with a plasma target.[19,21,48,49,59] Electrons accelerated in a plasma generate a large number of γ photons via nonlinear Compton scattering, and these photons interact with the strong field of the standing wave formed by the laser pulses from both directions. BW processes occur, and e^+e^- pairs are created.

In our case, two counterpropagating linearly p-polarized laser pulses interact with a circular target lying at their common focal spot [Fig. 1(a)]. The target is composed of electrons and deuterium ions, and its diameter is 3 μm. The simulation box of dimensions $40\,\mu m \times 100\,\mu m$ is resolved with 1200×3000 cells, each containing 100 simulation particles. As the two counterpropagating laser pulses overlap, a transient standing wave is created. The electrons oscillating in the electromagnetic standing wave serve as a source of γ photons. These emitted photons then interact with photons of the laser field, which results in e^+e^- pair creation via the BW process. For a given laser pulse, there exists an optimal initial target density such that the maximum number of seed electrons remain in the focal spot until the highest intensity of the standing wave is established. In our case, the highest number of positrons created per seed particle is achieved when a target of initial density $50n_{\text{cr}}$ ($200n_{\text{cr}}$) is used for the interaction with two colliding laser pulses having duration 15 fs (150 fs). Since both pulses have the same peak intensity, the longer one delivers more energy, which leads to more efficient positron production. In this case, 0.01 positrons per seed electron are created, while in the case of a short pulse, the number of positrons is ten times lower. The absolute number of created photons and positrons is much higher in the case of a longer laser pulse [Table I and Fig. 1(b)]. This is due to the four times higher number of seed particles and also to the much longer duration of the established standing wave. Therefore, a greater fraction of the laser energy is converted into photons and positrons in the long-pulse case. The probability of pair production depends on both the magnitude of the electric field and the photon momentum, as well as on their mutual orientation. Since the intensity and the mean photon energy are comparable in both cases, the mean positron energy is expected to be
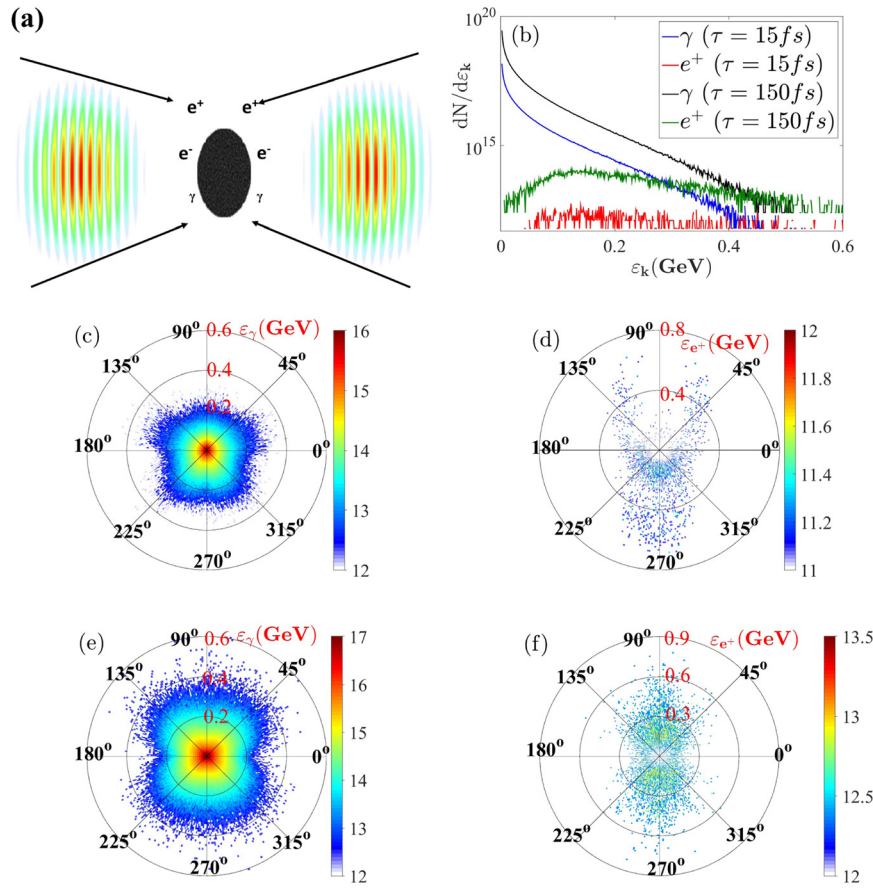
FIG. 1. Simulation results for two colliding laser pulses. (a) Schematic setup of the two-pulse collision regime. (b) Energy spectra for γ photons and positrons in both long- and short-pulse cases. (c) and (d) Angular distributions of energy for γ photons and positrons generated in the short-pulse case. (e) and (f) Corresponding results for the long-pulse case.

similar for both laser pulse durations (Table I). The angular distributions of the created photons are quite broad in both cases [Figs. 1(c) and 1(e)]. As the electric field of the standing wave oscillates in the direction of the laser pulse polarization, the created positrons are accelerated predominantly in this direction, as shown in Figs. 1(d) and 1(f). As the number of created positrons is much lower in the case of a shorter laser pulse, the actual phase of the oscillating standing wave is more pronounced in Fig. 1(d), resulting in an asymmetric distribution. After one-half of a laser period later, the electric field of the standing wave will acquire the opposite phase, and consequently will push positrons in the upward direction.

B. Single laser with plasma mirror reflection

In one of the pioneering works on hard X-ray emission via nonlinear Thomson scattering, Phuoc *et al.*[11] proposed a regime

TABLE I. Main simulation results for all setups: $\langle \epsilon_\gamma \rangle$ and $\langle \epsilon_{e^+} \rangle$ are the average energies of the γ photons and positrons; N_γ and N_{e^+} are the numbers of γ photons and positrons produced in the simulation box; η_γ and η_{e^+} are the laser energy conversion efficiencies to γ photons and positrons.

Setup[a]	$\langle \epsilon_\gamma \rangle$ (GeV)	N_γ (m^{-1})	η_γ (%)	$\langle \epsilon_{e^+} \rangle$ (GeV)	N_{e^+} (nC μm^{-1})	η_{e^+} (%)
A: $\tau = 15$fs	0.014	6.4×10^{18}	8.44	0.24	0.09	0.01
A: $\tau = 150$ fs	0.012	1.1×10^{20}	12.4	0.2	3.28	0.04
B: $\tau = 15$ fs	0.02	1.36×10^{19}	21	0.23	1.4	0.2
B: $\tau = 150$ fs	0.01	10^{20}	9.8	0.2	2	0.03

[a]A and B refer to the regimes of multicolliding laser pulses and of a single laser with plasma mirror reflection, discussed in Secs. III A and III B, respectively.

employing a solid target serving as the reflection mirror at the end of a gas target. Here, we demonstrate the possibility of using the reflection mirror for enhancing the nonlinear Compton scattering and the BW process, which are discussed in detail in Refs. 45 and 52. The simulation box has size $60\lambda \times 40\lambda$, with a resolution of 100 cells per λ. As can be seen in Fig. 2(a), the target is composed of a near-critical-density (NCD) plasma and an ultrathin solid layer. The NCD target has a density of $4n_{cr}$ and is 40λ in size. The main mechanism of electron acceleration depends on the target density. At NCD, direct laser acceleration dominates. The electrons are accelerated by the laser field, reaching the GeV level in a short distance. The solid target reflects the laser field, serving as a relativistic oscillating mirror. The solid target consists of a gold ion layer with a charge state of 11+ and free electrons with a corresponding density of $600n_{cr}$. The thickness of the target is 4λ. With the Doppler shift and self-focusing effects, the reflected intensity can be enhanced significantly. There is a head-on collision geometry between the reflected laser field and the high-energy accelerated electrons. The corresponding probabilities for nonlinear Compton scattering and the BW process become higher than in the case of electron self-injection.[18]

The spectrum in Fig. 2(b) indicates that the number of emitted γ photons in the $\tau = 150$ fs case (black) is larger than that in the $\tau = 15$ fs case (blue). However, the short-pulse case provides more high-frequency photons, and the cutoff energy reaches more than 1.5 GeV. The long pulse accelerates more electrons, since it occupies a much larger spatial area compared with the short pulse. Therefore, more electrons have the chance to emit γ photons. On the other hand, the laser ponderomotive force is inversely proportional to pulse length. A stronger ponderomotive force is applied to the electrons in the $\tau = 15$ fs case and accelerates them to higher energy. This can be seen from the tail of the γ-photon distribution function. The total numbers of photons in the long- and short-pulse cases are 10^{20} μm^{-1} and 1.4×10^{19} μm^{-1}, respectively. The distribution functions of the positrons for the two cases show similar tendencies. The total number of positrons in the long-pulse case is 2 nC μm^{-1}, with a cutoff energy of about 1 GeV. The number of positrons in the short-pulse case is slightly lower, 1.4 nC μm^{-1}. On the other hand, the maximum energy increases to about 1.5 GeV.

The angular distributions of energy for the γ photons and the positrons are presented in Figs. 2(c)–2(f). In the short-pulse case, both
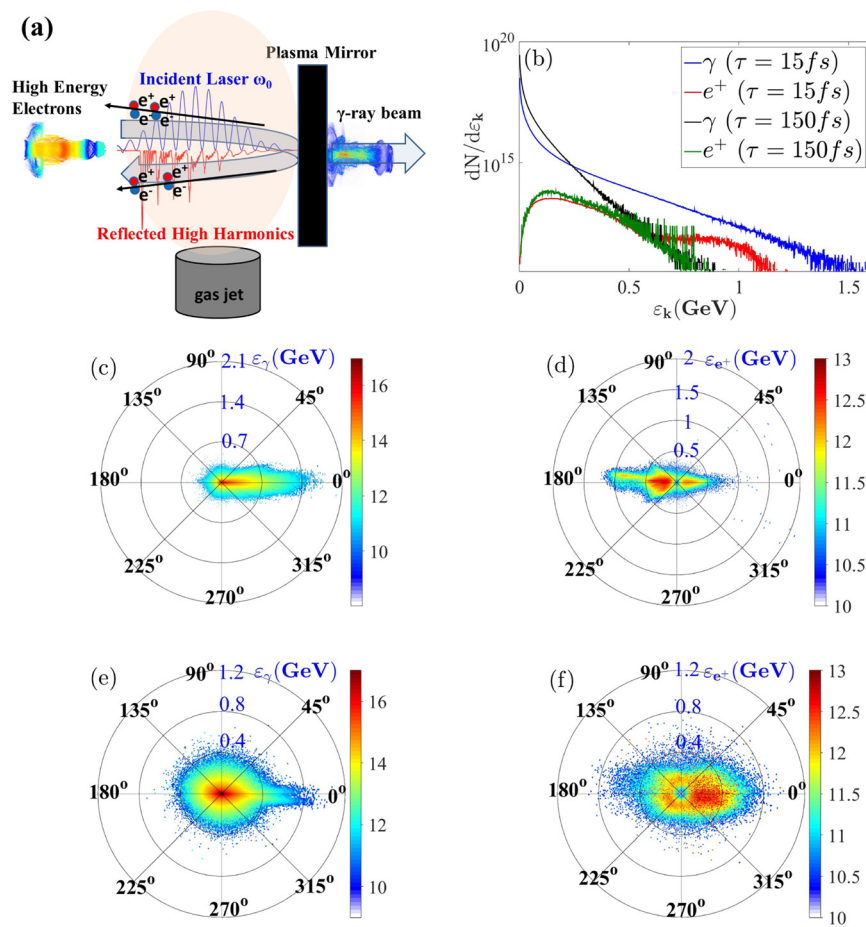

FIG. 2. Simulation results for a single laser pulse with a plasma mirror. (a) Schematic setup of the regime. (b) Energy spectra for γ photons and positrons in both long- and short-pulse cases. (c) and (d) Angular distributions of energy for γ photons and positrons generated in the short-pulse case. (e) and (f) Corresponding results for the long-pulse case.

the photons and the positrons are well collimated, with a narrow opening angle. However, the long-pulse results present a broadened and isotropic distribution of both γ photons and positrons, as can be seen in Figs. 2(e) and 2(f). The difference in beam quality comes from the field reflected by the plasma mirror. The solid target pushed by the incident pulse reflects the EM field via the relativistic oscillations of the electrons around the ion layer. The velocity of the ion layer (also called the piston velocity in the piston model) can be estimated by balancing the radiation momentum flux and the charged-particle momentum flux. Under the density conditions considered here, the velocity β_f is of the order of $0.1c$. The corresponding reflection process is regular in the short-pulse case owing to the minor displacement of the ion layer, $\delta s \sim \tau\beta_f \sim 0.5\lambda$. However, the long pulse significantly distorts the solid target, with a displacement as large as 5λ. Therefore, the long pulse is not favorable to being reflected by a plasma mirror in the high-intensity regime. Despite the fact that it provides relatively high numbers of γ photons and positrons, the energy and the beam quality are not comparable to those obtained in the short-pulse case.

IV. COMPARISON OF THE SCHEMES

In this section, we compare the simulation results obtained in the different regimes described above. The mean energy, the number of secondary particles and the laser energy conversion efficiency are summarized and compared in Table I. The mean energy of the γ photons and e^+e^- pairs are similar in all of the setups, which indicates that the mean energy is related to the amplitude of the laser field instead of the total energy. It should be mentioned that the energy of the positrons in the case with the plasma mirror and short laser pulse can be greatly enhanced in the later stage, since the positrons are captured by the reflected field, experiencing further acceleration during their propagation. The longer pulses provide a higher number of secondary particles. In the case of a standing wave formed by two colliding laser pulses, the use of long pulses is preferable, since it increases the spatial area occupied by the strong field of the standing wave. The production rates for both γ photons and positrons are much higher with the long pulse. However, in the setup using a single pulse and a plasma mirror, the simulation results show the opposite behavior. Although the absolute number is lower, the efficiencies are much higher with $\tau = 15$ fs. The main reason for this is the destruction of the plasma mirror by the long pulse, which reduces the reflection efficiency and collimation. For a given incident laser energy, the short pulse with a plasma mirror provides the highest production rate for γ photons and positrons. The beam qualities presented above are the best results for this regime too.

In conclusion, for the generation of γ photons and e^+e^- pairs with longer petawatt laser pulses, the standing wave configuration formed by two counterpropagating laser pulses provides better results in terms of the laser energy transformation efficiency. This results in the highest number of e^+e^- pairs being created in this configuration. For shorter petawatt laser pulses, the plasma mirror setup is beneficial, since it significantly enhances the production rate by more efficient laser pulse reflection and focusing. Furthermore, it provides the ideal beam qualities for further utilization of the γ-ray flash and the positron beam. The laser parameters discussed in this paper may be attained at upcoming facilities like ELI-Beamlines,[4] and thus these results are useful for designing future experiments.

REFERENCES

[1] A. D. Strickland and G. Mourou, "Compression of amplified chirped optical pulses," Opt. Commun. **56**, 219 (1985).

[2] V. Yanovsky et al., "Ultra-high intensity- 300-TW laser at 0.1 Hz repetition rate," Opt. Express **16**, 2109 (2008).

[3] A. S. Pirozhkov et al., "Approaching the diffraction-limited, bandwidth-limited petawatt," Opt. Express **25**, 20486 (2017).

[4] G. Mourou, G. Korn, W. Sandner, and J. Collier, *ELI Extreme Light Infrastructure (Whitebook)* (THOSS Media GmbH, Berlin, Germany, 2011).

[5] G. Chériaux et al., "Apollon-10p: Status and implementation," AIP Conf. Proc. **1462**, 78 (2012).

[6] C. Bamber et al., "Studies of nonlinear QED in collisions of 46.6 GeV electrons with intense laser pulses," Phys. Rev. D **60**, 092004 (1999).

[7] A. R. Bell and J. G. Kirk, "Possibility of prolific pair production with high-power lasers," Phys. Rev. Lett. **101**, 200403 (2008).

[8] I. V. Sokolov, N. M. Naumova, J. A. Nees, and G. A. Mourou, "Pair creation in QED-strong pulsed laser fields interacting with electron beams," Phys. Rev. Lett. **105**, 195005 (2010).

[9] S. S. Bulanov, V. D. Mur, N. B. Narozhny, J. Nees, and V. S. Popov, "Multiple colliding electromagnetic pulses: A way to lower the threshold of e^+e^- pair production from vacuum," Phys. Rev. Lett. **104**, 220404 (2010).

[10] A. A. Gonoskov, A. V. Korzhimanov, A. V. Kim, M. Marklund, and A. M. Sergeev, "Ultrarelativistic nanoplasmonics as a route towards extreme-intensity attosecond pulses," Phys. Rev. E **84**, 046403 (2011).

[11] K. T. Phuoc et al., "All-optical Compton gamma-ray source," Nat. Photonics **6**, 308 (2012).

[12] T. Nakamura et al., "High-power γ-ray flash generation in ultraintense laser-plasma interactions," Phys. Rev. Lett. **108**, 195001 (2012).

[13] C. P. Ridgers et al., "Dense electron-positron plasmas and ultraintense γ rays from laser-irradiated solids," Phys. Rev. Lett. **108**, 165006 (2012).

[14] L. L. Ji, A. Pukhov, I. Y. Kostyukov, B. F. Shen, and K. Akli, "Radiation-reaction trapping of electrons in extreme laser fields," Phys. Rev. Lett. **112**, 145003 (2014).

[15] T. G. Blackburn, C. P. Ridgers, J. G. Kirk, and A. R. Bell, "Quantum radiation reaction in laser–electron-beam collisions," Phys. Rev. Lett. **112**, 015001 (2014).

[16] X.-L. Zhu et al., "Enhanced electron trapping and γ ray emission by ultra-intense laser irradiating a near-critical-density plasma filled gold cone," New J. Phys. **17**, 053039 (2015).

[17] X. Ribeyre et al., "Pair creation in collision of γ-ray beams produced with high-intensity lasers," Phys. Rev. E **93**, 013201 (2016).

[18] Y. J. Gu, O. Klimo, S. Weber, and G. Korn, "High density ultrashort relativistic positron beam generation by laser-plasma interaction," New J. Phys. **18**, 113023 (2016).

[19] H.-Z. Li et al., "Ultra-bright gamma-ray emission and dense positron production from two laser-driven colliding foils," Sci. Rep. **7**, 17312 (2017).

[20]H. X. Chang *et al.*, "Brilliant petawatt gamma-ray pulse generation in quantum electrodynamic laser-plasma interaction," Sci. Rep. **7**, 45031 (2017).

[21]X.-L. Zhu *et al.*, "Dense GeV electron-positron pairs generated by lasers in near-critical-density plasmas," Nat. Commun. **7**, 13686 (2016).

[22]Z. Gong *et al.*, "Brilliant GeV gamma-ray flash from inverse Compton scattering in the QED regime," Plasma Phys. Controlled Fusion **60**, 044004 (2018).

[23]M. Jirka, O. Klimo, M. Vranic, S. Weber, and G. Korn, "QED cascade with 10 PW-class lasers," Sci. Rep. **7**, 15302 (2017).

[24]T. G. Blackburn and M. Marklund, "Nonlinear Breit-Wheeler pair creation with bremsstrahlung γ rays," Plasma Phys. Controlled Fusion **60**(5), 054009 (2018).

[25]G. A. Mourou, T. Tajima, and S. V. Bulanov, "Optics in the relativistic regime," Rev. Mod. Phys. **78**, 309 (2006).

[26]A. Di Piazza, K. Z. Hatsagortsyan, and C. H. Keitel, "Strong signatures of radiation reaction below the radiation-dominated regime," Phys. Rev. Lett. **102**, 254802 (2009).

[27]A. Di Piazza, C. Müller, K. Z. Hatsagortsyan, and C. H. Keitel, "Extremely high-intensity laser interactions with fundamental quantum systems," Rev. Mod. Phys. **84**, 1177 (2012).

[28]S. V. Bulanov, "Magnetic reconnection: From MHD to QED," Plasma Phys. Controlled Fusion **59**, 014029 (2017).

[29]J. M. Cole *et al.*, "Experimental evidence of radiation reaction in the collision of a high-intensity laser pulse with a laser-wakefield accelerated electron beam," Phys. Rev. X **8**, 011020 (2018).

[30]K. Poder *et al.*, "Experimental signatures of the quantum nature of radiation reaction in the field of an ultraintense laser," Phys. Rev. X **8**, 031004 (2018).

[31]J. Galy, M. Maucec, D. J. Hamilton, R. Edwards, and J. Magill, "Bremsstrahlung production with high-intensity laser matter interactions and applications," New J. Phys. **9**, 23 (2007).

[32]K. W. D. Ledingham and W. Galster, "Laser-driven particle and photon beams and some applications," New J. Phys. **12**, 045005 (2010).

[33]Y. Glinec *et al.*, "High-resolution γ-ray radiography produced by a laser-plasma driven electron source," Phys. Rev. Lett. **94**, 025003 (2005).

[34]A. Giulietti *et al.*, "Intense γ-ray source in the giant-dipole-resonance range driven by 10-TW laser pulses," Phys. Rev. Lett. **101**, 105002 (2008).

[35]J. Vyskočil, O. Klimo, and S. Weber, "Simulations of bremsstrahlung emission in ultra-intense laser interactions with foil targets," Plasma Phys. Controlled Fusion **60**, 054013 (2018).

[36]G. Sarri *et al.*, "Ultrahigh brilliance multi-MeV γ-ray beams from nonlinear relativistic Thomson scattering," Phys. Rev. Lett. **113**, 224801 (2014).

[37]D. J. Stark, T. Toncian, and A. V. Arefiev, "Enhanced multi-MeV photon emission by a laser-driven electron beam in a self-generated magnetic field," Phys. Rev. Lett. **116**, 185003 (2016).

[38]W. Yan *et al.*, "High-order multiphoton Thomson scattering," Nat. Photonics **11**, 514 (2017).

[39]B. Martinez, E. d'Humières, and L. Gremillet, "Synchrotron emission from nanowire array targets irradiated by ultraintense laser pulses," Plasma Phys. Controlled Fusion **60**, 074009 (2018).

[40]W. M. Wang, Zh. M. Sheng, P. Gibbon, L. M. Chen, Y. T. Li, and J. Zhang, "Collimated ultrabright gamma rays from electron wiggling along a petawatt laser-irradiated wire in the QED regime," Proc. Natl. Acad. Sci. U. S. A. **115**, 9911 (2018).

[41]C. Bula *et al.*, "Observation of nonlinear effects in Compton scattering," Phys. Rev. Lett. **76**, 3116 (1996).

[42]A. Di Piazza, K. Z. Hatsagortsyan, and C. H. Keitel, "Quantum radiation reaction effects in multiphoton Compton scattering," Phys. Rev. Lett. **105**, 220403 (2010).

[43]A. Benedetti, M. Tamburini, and C. H. Keitel, "Giant collimated gamma-ray flashes," Nat. Photonics **12**, 319 (2018).

[44]X. L. Zhu *et al.*, "Bright attosecond γ-ray pulses from nonlinear Compton scattering with laser-illuminated compound targets," Appl. Phys. Lett. **112**, 174102 (2018).

[45]Y. J. Gu and S. Weber, "Intense, directional and tunable γ-ray emission via relativistic oscillaitng plasma mirror," Opt. Express **26**, 19932 (2018).

[46]G. Breit and J. A. Wheeler, "Collision of two light quanta," Phys. Rev. **46**, 1087 (1934).

[47]A. I. Nikishov and V. I. Ritus, "Interaction of electrons and photons with a very strong electromagnetic field," Sov. Phys. - Usp. **13**, 303 (1970).

[48]M. Jirka *et al.*, "Electron dynamics and γ and e^-e^+ production by colliding laser pulses," Phys. Rev. E **93**, 023207 (2016).

[49]M. Tamburini, A. D. Piazza, and C. H. Keitel, "Laser-pulse-shape control of seeded QED cascades," Sci. Rep. **7**, 5694 (2017).

[50]O. Jansen *et al.*, "Leveraging extreme laser-driven magnetic fields for gamma-ray generation and pair production," Plasma Phys. Controlled Fusion **60**, 054006 (2018).

[51]M. Vranic, O. Klimo, G. Korn, and S. Weber, "Multi-GeV electron-positron beam generation from laser-electron scattering," Sci. Rep. **8**, 4702 (2018).

[52]Y.-J. Gu, O. Klimo, S. V. Bulanov, and S. Weber, "Brilliant gamma-ray beam and electron-positron pair production by enhanced attosecond pulses," Commun. Phys. **1**, 93 (2018).

[53]S. V. Bulanov *et al.*, "On some theoretical probels of laser wake-field accelerators," J. Plasma Phys. **82**, 905820308 (2016).

[54]C. Gahn *et al.*, "Multi-MeV electron beam generation by direct laser acceleration in high-density plasma channels," Phys. Rev. Lett. **83**, 4772 (1999).

[55]S. V. Bulanov *et al.*, "On the problems of relativistic laboratory astrophysics and fundamental physics with super powerful lasers," Plasma Phys. Rep. **41**, 1 (2015).

[56]L. Landau and E. Lifshitz, *The Classical Theory of Fields*, Volume 2 of Course of Theoretical Physics, 4th ed. (Pergamon, Amsterdam, 1975).

[57]C. Ridgers *et al.*, "Modelling gamma-ray photon emission and pair production in high-intensity laser–matter interactions," J. Comput. Phys. **260**, 273 (2014).

[58]T. D. Arber *et al.*, "Contemporary particle-in-cell approach to laser-plasma modelling," Plasma Phys. Controlled Fusion **57**, 113001 (2015).

[59]W. Luo *et al.*, "Dense electron-positron plasmas and gamma-ray bursts generation by counter-propagating quantum electrodynamics-strong laser interaction with solid targets," Phys. Plasmas **22**, 063112 (2015).